Rock and Soil Mechanics

Volume 43 | Issue 8 Article 6

10-9-2022

Analytical method to estimate the influence of foundation pit excavation adjacent to the station (working shaft) on the underlying shield tunnel

Zu-xian WANG
School of Civil Engineering, Central South University, Changsha, Hunan 410075, China

Cheng-hua SHI
School of Civil Engineering, Central South University, Changsha, Hunan 410075, China

Chen-jie GONG
School of Civil Engineering, Central South University, Changsha, Hunan 410075, China,
gongcj@csu.edu.cn

Cheng-yong CAO
College of Civil and Transportation Engineering, Shenzhen University, Shenzhen, Guangdong 518060, China

See next page for additional authors

Custom Citation

WANG Zu-xian, SHI Cheng-hua, GONG Chen-jie, CAO Cheng-yong, LIU Jian-wen, PENG Zhu, . Analytical method to estimate the influence of foundation pit excavation adjacent to the station (working shaft) on the underlying shield tunnel[J]. Rock and Soil Mechanics, 2022, 43(8): 2176-2190.

Analytical method to estimate the influence of foundation pit excavation adjacent to the station (working shaft) on the underlying shield tunnel

Authors

Zu-xian WANG, Cheng-hua SHI, Chen-jie GONG, Cheng-yong CAO, Jian-wen LIU, and Zhu PENG

Rock and Soil Mechanics 2022 43(8): 2176−2190 ISSN 1000−7598
https: //doi.org/10.16285/j.rsm.2021.7108 rocksoilmech.researchcommons.org/journal

Analytical method to estimate the influence of foundation pit excavation adjacent to the station (working shaft) on the underlying shield tunnel

WANG Zu-xian[1], SHI Cheng-hua[1], GONG Chen-jie[1], CAO Cheng-yong[2], LIU Jian-wen[1], PENG Zhu[1]

1. School of Civil Engineering, Central South University, Changsha, Hunan 410075, China

2. College of Civil and Transportation Engineering, Shenzhen University, Shenzhen, Guangdong 518060, China

Abstract: The shield tunnel is typically simplified as an infinite beam with two free ends in existing analytical models, which are used to calculate the longitudinal deformation of the underlying shield tunnel induced by the excavation of a foundation pit. However, the applicability of those analytical models is limited due to the simplification. The current study is aimed at estimating analytically the longitudinal deformation of the underlying shield tunnel induced by the excavation of a foundation pit adjacent to the station (working shaft). The constraint on the shield tunnel generated by the joint between the station (working shaft) and the tunnel is treated as a rotation spring with the rotation stiffness of K_θ and a vertical rod support. The Winkler foundation–Timoshenko beam model for calculating the longitudinal deformation of the shield tunnel adjacent to the station (working shaft) induced by the foundation pit excavation is proposed. The finite difference solution of the proposed model is strictly derived based on the basic principles of the force method. The reliability and applicability of the proposed analytical model are verified via the comparison with the finite element numerical solution of one-dimensional elastic foundation beam model and the global finite element simulation results of the longitudinal deformation of the underlying tunnel induced by the excavation of a foundation pit adjacent to the station. The parametric studies indicate the following conclusions. (i) The longitudinal deformation and internal forces of the shield tunnel are significantly influenced by the rotation stiffness, K_θ, of the joint between the station (working shaft) and the tunnel. The internal forces and the longitudinal deformation (i.e. rotation angle) at the end of the tunnel increase and decreases nonlinearly with a increasing K_θ, respectively. In addition, when the flexible connection is adopted at the joint between the station (working well) and tunnel, the working performance of the shield tunnel at the joint can be better guaranteed. (ii) The constraint effect of the joint on the end of the tunnel is non-negligible, when the distance from the center of the foundation pit to the station-tunnel joint ranges from 4 to 5 times the width of the pit along the tunnel axis. In this condition, the proposed analytical model should be adopted to evaluate the longitudinal working performance of the tunnel. (iii) The influence of the overlying foundation pit excavation on the underlying tunnel mainly exerts within 2 times the length of the pit perpendicular to the tunnel axis away from the center of the pit.

Keywords: shield tunnel; foundation pit excavation; flexible boundary; longitudinal deformation; analytical solution

1 Introduction

Longitudinal uneven deformation is an important factor, which induces various types of damages of the lining of shield tunnels. The remarkable differential settlement of tunnels will cause unfavorable consequences, such as the dislocation of segments, joint opening, and lining cracking, which further lead to the failure of the waterproof and the structures of the lining and influence the working performance of shield tunnels[1–3]. As the urban underground space develops, the issues related to the longitudinal deformation of shield tunnels caused by various unfavorable conditions has become increasingly serious, mainly including the excavation of adjacent foundation pits[4–9], the construction of new tunnels[10–14] and sudden surcharge on the ground[15–17].

Extensive studies on the longitudinal deformation of shield tunnels have been conducted, a considerable part of which focused on analytical models for estimating the longitudinal mechanical properties of shield tunnels under the influence of various unfavorable conditions of loading and unloading[18]. From the mechanical point of view, those models share the same underlying essence, namely the shield tunnel–soil interaction. Thus, whatever the working conditions are involved, the basic framework of most analytical models is the elastic foundation beam model, the core procedure of which is to describe the tunnel– soil interaction and to conduct the mechanical analysis of the shield tunnel structure.

The interaction between tunnel and soil is typically described by various foundation models, such as Winkler foundation model, Pasternak foundation model, Vlazov foundation model with two parameters and Kerr foundation model with three parameters. Although those two-parameter and three-parameter foundation models theoretically overcome the drawback of the Winkler foundation model associated with the discontinuity[19], it is difficult to determine the model parameters and to apply those models in practice. The Winkler foundation mode is the most widely used for estimating the structure–soil interaction, because of its advantages such as the few model parameters, easy to determinate, convenient to estimate and input into the model[20].

Received: 28 November 2021 Revised: 24 June 2022
This work was supported by the National Natural Science Foundation of China (51908557, 51778636) and the Natural Science Foundation of Hunan Province (2021JJ30837).
First author: WANG Zu-xian, male, born in 1994, PhD candidate, mainly engaged in research on tunnel and underground engineering. E-mail: csusdwzx@csu.edu.cn
Corresponding author: GONG Chen-jie, male, born in 1990, PhD, Professor, mainly engaged in teaching and scientific research on shield tunnel structure safety. E-mail: gongcj@csu.edu.cn

The longitudinal structure analysis of shield tunnels is typically based on the longitudinal beam–spring model[21] and the equivalent longitudinal continuous model[22]. Therefore, numerous analytical models can be developed by combining different foundation models and the longitudinal structure analysis theory of shield tunnels. In comparison to the longitudinal beam–spring model, the equivalent longitudinal continuous model has a simpler concept, a more convenient model input and solving strategy. Thus, a one-dimensional homogeneous continuous beam on an elastic foundation has become the most popular model for estimating the structural response of shield tunnels under the additional loads.

With a better understanding of the longitudinal deformation mode of shield tunnels, Timoshenko beam theory has been introduced for modelling the longitudinal deformation of shield tunnels, which can consider both bending and shear effects[23]. Thus, the research progress on this topic has been promoted. The longitudinal deformation model of shield tunnels based on Timoshenko beam theory has been widely used for modelling the structural responses of shield tunnels under various types of additional loads. For example, Liang[5–6] established the Winkler foundation–Timoshenko beam model[5] and the Pasternak foundation–Timoshenko beam model[6] for modelling the influence of foundation pit construction on the adjacent shield tunnel. Liu et al.[7–8] further considered the influence of foundation pit construction on foundation parameters and established the Vlazov foundation–Timoshenko beam model for modelling the longitudinal additional responses of the shield tunnel induced by the foundation pit construction. Zhang et al.[12–13] established the Kerr foundation–Timoshenko beam model and investigated the influence of the new tunnel construction on existing shield tunnels. Kang et al.[16] analyzed the effect of the surcharge on the ground surface on existing shield tunnels based on the Winkler foundation–Timoshenko beam model.

It should be pointed out that the existing studies typically model the shield tunnel as an infinite beam on an elastic foundation. In addition, the two ends of the shield tunnel are typically simplified as free ends to facilitate the derivation of the finite difference equation if the finite difference method is used. However, as for the joints between the interval tunnels and the station or the air shaft, this simplification is not valid when there are additional loads acting on the shield tunnel adjacent to those joints. Under this condition, the joint between the working shaft and the shield tunnel has remarkable constraint effect on the tunnel ends. Thus, the significant error will be introduced to the modelling results of the longitudinal response of shield tunnels based on the free end assumption. Wu et al.[24] proposed the rigorous analytical solutions of the Vlazov foundation–Timoshenko beam model under two types of boundary conditions and the external loads with the expansion of Fourier series. However, the governing equation of this type of problems is generally a fourth order non-homogeneous differential equation. When the external load and foundation parameters vary along the longitudinal direction of the tunnel, it is difficult to obtain the rigorous analytical solution mathematically.

The current study aims at the longitudinal deformation of the underlying shield tunnel induced by the excavation of the foundation pit adjacent to the station (working shaft). The Winkler foundation–Timoshenko beam model was used for the longitudinal structure analysis of the shield tunnel. The calculation model for the longitudinal shield tunnel under the condition of unloading due to the excavation adjacent to the station (working shaft) was established, which considered the constraint effect of the station (working shaft) on the end of the shield tunnel. Based on the principle of force method, the finite difference solution of the longitudinal response of shield tunnel under complicated boundary condition was derived. The proposed model is capable to extending the applicability of the existing models for estimating the longitudinal deformation of shield tunnels. Moreover, the modelling results provide the referable solutions for the elastic foundation beam model under the complicated boundary conditions by the finite difference method and for the rational design of the joint between the station (working shaft) and the shield tunnel.

2 Winkler foundation–Timoshenko beam model

2.1 Station (working shaft)–shield tunnel analytical model

Figure 1 illustrates the calculation model for analytically solving the additional response of the underlying shield tunnel caused by the excavation of a foundation pit adjacent to the station (working shaft)-shield tunnel joint. Timoshenko beam model is used to simulate the mechanical behavior of the shield tunnel including the longitudinal deformation. The interaction

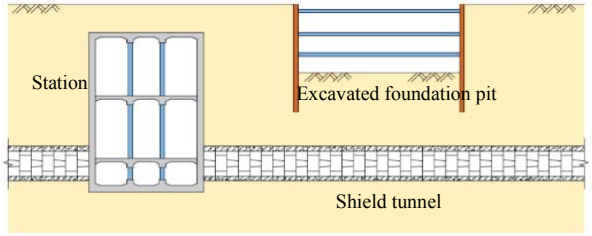

(a) Schematical illustration of the excavated foundation pit adjacent to a station (working shaft)

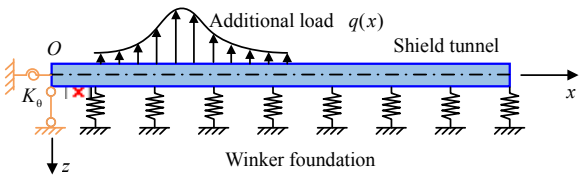

(b) Winkler foundation–Timoshenko beam model

Fig. 1 Schematic illustration for the calculation model of the longitudinal deformation of the shield tunnel adjacent to the station (working shaft)

between the shield tunnel and the surrounding soils is modelled by the Winkler foundation model. According to the research results by Wu et al.[22], the station (working shaft)-shield tunnel joint can be modelled by the combination of a rotation spring with a rotational stiffness of K_θ and a vertically simple support, which can be regarded as a simply supported flexible constraint.

2.2 Governing equations

For the Winkler foundation model, the relationship between the earth pressure $p(x)$ and the displacement $w(x)$ at any point of the foundation can be expressed as

$$p(x) = kw(x) \tag{1}$$

where k is the coefficient of subgrade reaction.

According to Timoshenko beam theory, the relationship between deformation and internal forces are expressed in the differential form[25]:

$$M = -D\frac{\mathrm{d}\varphi}{\mathrm{d}x} \tag{2}$$

$$Q = C\left(\frac{\mathrm{d}w}{\mathrm{d}x} - \varphi\right) \tag{3}$$

where M and Q are bending moment and shear force acting on the given cross-section of beam, respectively; $D = EI$ is the bending stiffness of the beam, which is the longitudinal equivalent bending stiffness for the shield tunnel, $(EI)_{\mathrm{eq}}$; E is the Young's modulus of elasticity of the beam; I is the moment of inertia of the cross-section of the beam; $C = \kappa GA$ is the shear stiffness of beam cross-section, which is the equivalent shear stiffness for the shield tunnel, $(\kappa GA)_{\mathrm{eq}}$; κ is the correction coefficient; G is the shear modulus of the beam; A is the area of beam cross-section; φ is the angle of rotation of the beam cross-section; and w is the deflection of the beam.

Considering the beam segment with the length of dx in Fig. 1(b), the force equilibrium diagram is shown in Fig. 2. Thus, the force equilibrium equations can be written as

$$Q + \mathrm{d}Q + qD_{\mathrm{t}}\mathrm{d}x = Q + pD_{\mathrm{t}}\mathrm{d}x \tag{4}$$

$$M + Q\mathrm{d}x + pD_{\mathrm{t}}\frac{(\mathrm{d}x)^2}{2} = M + \mathrm{d}M + qD_{\mathrm{t}}\frac{(\mathrm{d}x)^2}{2} \tag{5}$$

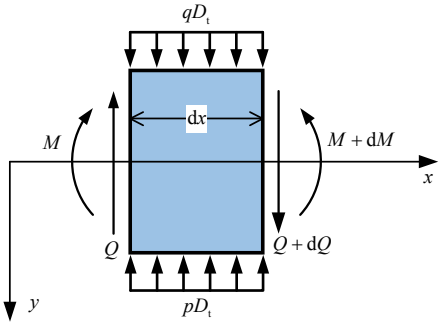

Fig. 2 Force equilibrium diagram for the soil beam element

where D_{t} is the outer diameter of the shield tunnel; and q is the external load.

By combining Eq. (1) to Eq. (5), omitting high-order terms and assuming that $K = kD_{\mathrm{t}}$, the rotation angle φ and the deflection w of a Timoshenko beam on a Winkler foundation subjected to an external load can be obtained by the differential equilibrium equations

$$\frac{\mathrm{d}}{\mathrm{d}x}\left[C\left(\frac{\mathrm{d}w}{\mathrm{d}x} - \varphi\right)\right] = Kw - qD_{\mathrm{t}} \tag{6}$$

$$-D\frac{\mathrm{d}^2\varphi}{\mathrm{d}x^2} = C\left(\frac{\mathrm{d}w}{\mathrm{d}x} - \varphi\right) \tag{7}$$

By decoupling Eq. (6) and Eq. (7), the differential governing equations of the responses of a Timoshenko beam on a Winkler foundation subjected to an additional load can be rewritten as

$$\frac{\mathrm{d}^4w}{\mathrm{d}x^4} - \frac{K}{C}\frac{\mathrm{d}^2w}{\mathrm{d}x^2} + \frac{K}{D}w = \frac{D_{\mathrm{t}}}{D}q - \frac{D_{\mathrm{t}}}{C}\frac{\mathrm{d}^2q}{\mathrm{d}x^2} \tag{8}$$

2.3 Finite difference solution

Equation (8) is a fourth order non-homogeneous differential equation. It is difficult to find its exact solution. For the convenience of engineering application, the finite difference method can be used to find its numerically approximated solution. In addition, the finite difference solution is more adaptive than the analytical solution, when the additional load or the foundation parameters varies along the longitudinal direction of the tunnel. As shown in Fig. 3, the shield tunnel is discretized into $n+5$ nodes along the longitudinal direction of the tunnel (including two extra virtual nodes at both ends) with the element length of l.

According to the standard finite difference principle, the differential governing equation (i.e., Eq. (8)) can be approximated by the following difference equation

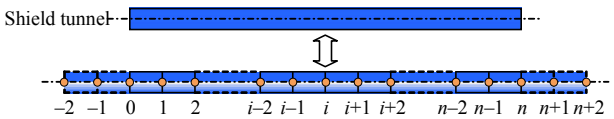

Fig. 3 Spatial discretization of the shield tunnel

$$\frac{6w_i - 4(w_{i+1} + w_{i-1}) + (w_{i+2} + w_{i-2})}{l^4} - \frac{K}{C}\frac{w_{i+1} - 2w_i + w_{i-1}}{l^2} + \frac{K}{D}w_i = \frac{D_{\mathrm{t}}}{D}q_i - \frac{D_{\mathrm{t}}}{C}\frac{q_{i+1} - 2q_i + q_{i-1}}{l^2} \tag{9}$$

From Eq. (9), $n+1$ independent equations with $n+5$ unknowns are obtained. The four complementary equations are determined by the boundary conditions at both ends of the tunnel, which are the nodal displacements of the four virtual nodes.

Let $\alpha_1=\frac{1}{l^4}$, $\alpha_2=\frac{K}{Cl^2}$, $\alpha_3=\frac{K}{D}$, $\alpha_4=\frac{D_t}{D}$, and $\alpha_5=\frac{D_t}{Cl^2}$. Eq. (9) can be written in the matrix form as

$$\boldsymbol{w}=(\boldsymbol{K}_1-\boldsymbol{K}_2+\boldsymbol{K}_3)^{-1}(\boldsymbol{Q}_1-\boldsymbol{Q}_2-\boldsymbol{Q}_3) \tag{10}$$

where $\boldsymbol{w}$ is the column vector of the tunnel nodal displacements; $\boldsymbol{K}_1$ is the displacement stiffness matrix of the tunnel; $\boldsymbol{K}_2$ is the shear stiffness matrix of the tunnel; $\boldsymbol{K}_3$ is the bending stiffness matrix of the tunnel; $\boldsymbol{Q}_1$ is the column vector of the additional load; $\boldsymbol{Q}_2$ is the column vector of the load correction; and $\boldsymbol{Q}_3$ is the complementary vector. The $\boldsymbol{K}_1$, $\boldsymbol{K}_2$, and $\boldsymbol{Q}_3$ need to be determined according to the nodal displacements of the virtual nodes. $\boldsymbol{K}_3$, $\boldsymbol{w}$, $\boldsymbol{Q}_1$, and $\boldsymbol{Q}_2$ can be expressed as

$$\left.\begin{aligned}
\boldsymbol{K}_3&=\begin{bmatrix}1&&&&\\&1&&&\\&&\ddots&&\\&&&1&\\&&&&1\end{bmatrix}_{(n+1)\times(n+1)}\\
\boldsymbol{w}&=\{w_0,\ w_1,\ \cdots,\ w_{n-1},\ w_n\}^{\mathrm{T}}_{1\times(n+1)}\\
\boldsymbol{Q}_1&=\alpha_4\{q_0,\ q_1,\ \cdots,\ q_{n-1},\ q_n\}^{\mathrm{T}}_{1\times(n+1)}\\
\boldsymbol{Q}_2&=\alpha_5\begin{Bmatrix}q_1-2q_0+q_{-1}\\q_2-2q_1+q_0\\\vdots\\q_n-2q_{n-1}+q_{n-2}\\q_{n+1}-2q_n+q_{n-1}\end{Bmatrix}_{(n+1)\times1}
\end{aligned}\right\} \tag{11}$$

According to Figs. 1(b) and 3, the boundary conditions at both ends of the tunnel, i.e., the nodal displacements of the virtual nodes in the analytical model are

$$\left.\begin{aligned}M_n&=0\\Q_n&=0\end{aligned}\right\} \tag{12}$$

In addition, in order to obtain the finite difference solution, the boundary conditions of the bending moment and shear force at the beam end adjacent to the station (working shaft) should be given.

The discretized beam segment between nodes $i=0$ and $i=1$ is taken as the research object, as shown in Fig. 4. According to the boundary conditions at the beam ends, the nodal displacement is null, and the rotation angle of the beam cross-section is φ_0 at node 0. At node 1 which is the discretization point, the longitudinal displacement of the beam is w_1, and the rotation angle of the beam cross-section is φ_1. As the external load acting on the beam segment between nodes 0 and 1, q_m is taken as the average value of the external loads acting at those two nodes.

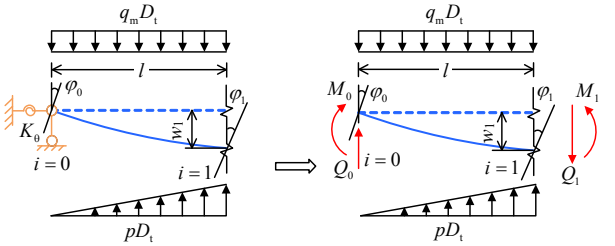

(a) The selected free body (b) Force method analysis of the free body

Fig. 4 Free body diagram for the discretized tunnel between nodes 0 and 1

According to Fig. 4, the basic equations for shear force Q_0 and bending moment M_0 at node 0 based on the force method are

$$\left.\begin{aligned}Q_0\delta_{11}+M_0\delta_{12}+\Delta_1^{\mathrm{P1}}+\Delta_1^{\mathrm{P2}}+l\varphi_1-w_1&=0\\Q_0\delta_{21}+M_0\delta_{22}+\Delta_2^{\mathrm{P1}}+\Delta_2^{\mathrm{P2}}+\varphi_1&=-\frac{M_0}{K_\theta}\end{aligned}\right\} \tag{13}$$

where δ_{11}, δ_{12}, Δ_1^{P1}, and Δ_1^{P2} are the displacement along the direction of Q_0 at node $i=0$ when the unit loads corresponding to Q_0 and M_0 act alone, the subgrade reaction (pD_t) acts alone, and the external load (q_mD_t) acts alone, respectively; and δ_{22}, δ_{21}, Δ_2^{P1}, and Δ_2^{P2} are the rotation angle along the direction of M_0 at node 0 when the unit load corresponding to Q_0 and M_0 act alone, the subgrade reaction (pD_t) acts alone, and the external load (q_mD_t) acts alone, respectively. Those terms can be obtained by the following formulas

$$\left.\begin{aligned}
\delta_{11}&=\int\frac{\bar{M}_1\bar{M}_1}{D}\mathrm{d}x=\frac{l^3}{3D}\\
\delta_{12}=\delta_{21}&=\int\frac{\bar{M}_1\bar{M}_2}{D}\mathrm{d}x=\frac{l^2}{2D}\\
\delta_{22}&=\int\frac{\bar{M}_2\bar{M}_2}{D}\mathrm{d}x=\frac{l}{D}\\
\Delta_1^{\mathrm{P1}}&=\int\frac{\bar{M}_1\bar{M}_{\mathrm{P1}}}{D}\mathrm{d}x=\frac{l^4}{30D}Kw_1\\
\Delta_1^{\mathrm{P2}}&=\int\frac{\bar{M}_1\bar{M}_{\mathrm{P2}}}{D}\mathrm{d}x=-\frac{q_mD_tl^4}{8D}\\
\Delta_2^{\mathrm{P1}}&=\int\frac{\bar{M}_2\bar{M}_{\mathrm{P1}}}{D}\mathrm{d}x=\frac{l^3}{24D}Kw_1\\
\Delta_2^{\mathrm{P2}}&=\int\frac{\bar{M}_2\bar{M}_{\mathrm{P2}}}{D}\mathrm{d}x=-\frac{q_mD_tl^3}{6D}
\end{aligned}\right\} \tag{14}$$

Moreover, it can be derived from Eq. (13) that

$$\left.\begin{aligned}
M_0&=\beta\left[\delta_{12}\left(\Delta_1^{\mathrm{P1}}+\Delta_1^{\mathrm{P2}}+l\varphi_1-w_1\right)-\right.\\
&\qquad\left.\delta_{11}\left(\Delta_2^{\mathrm{P1}}+\Delta_2^{\mathrm{P2}}+\varphi_1\right)\right]\\
Q_0&=\beta\left[\delta_{12}\left(\Delta_2^{\mathrm{P1}}+\Delta_2^{\mathrm{P2}}+\varphi_1\right)-\right.\\
&\qquad\left.\left(\delta_{22}+1/K_\theta\right)\left(\Delta_1^{\mathrm{P1}}+\Delta_1^{\mathrm{P2}}+l\varphi_1-w_1\right)\right]
\end{aligned}\right\} \tag{15}$$

where $\beta=\dfrac{1}{\delta_{11}\left(\delta_{22}+1/K_\theta\right)-\delta_{12}{}^2}$.

In addition, according to the differential equilibrium equations with respect to the rotation angle φ and the deflection w, the rotation angle φ, bending moment M and shear force Q of the tunnel can be obtained by the following standard finite difference form:

$$\left.\begin{aligned}
\varphi_i &= \frac{w_{i+1}-w_{i-1}}{2l}+\frac{D}{C}\left(\frac{w_{i+2}-2w_{i+1}+2w_{i-1}-w_{i-2}}{2l^3}-\right.\\
&\left.\frac{K}{C}\frac{w_{i+1}-w_{i-1}}{2l}+\frac{D_{\mathrm{t}}}{C}\frac{q_{i+1}-q_{i-1}}{2l}\right)\\
M_i &= -\frac{D}{C}\left(C\frac{w_{i+1}-2w_i+w_{i-1}}{l^2}-Kw_i+D_{\mathrm{t}}q_i\right)\\
Q_i &= -\frac{D}{C}\left(C\frac{w_{i+2}-2w_{i+1}+2w_{i-1}-w_{i-2}}{2l^3}-\right.\\
&\left.K\frac{w_{i+1}-w_{i-1}}{2l}+D_{\mathrm{t}}\frac{q_{i+1}-q_{i-1}}{2l}\right)
\end{aligned}\right\} \tag{16}$$

Combining Eqs. (12), (15) and (16), the displacements of the four virtual nodes at both ends of the tunnel can be calculated as

$$\left.\begin{aligned}
w_{-1} &= c_0w_0+c_1w_1+c_2w_2+c_3w_3+c_4q_0+c_5q_2+c_6q_{\mathrm{m}}\\
w_{-2} &= c_7w_{-1}+c_8w_0+c_9w_1+c_{10}w_2+c_{11}w_3+c_{12}q_{-1}+\\
&\quad c_{13}q_0+c_{14}q_1+c_{15}q_2+c_{16}q_{\mathrm{m}}\\
w_{n+1} &= c_{17}w_n-w_{n-1}-c_{14}q_n\\
w_{n+2} &= c_{17}w_{n+1}-c_{17}w_{n-1}+w_{n-2}+c_{14}\left(q_{n-1}-q_{n+1}\right)
\end{aligned}\right\} \tag{17}$$

where $c_0=\dfrac{Kl^2}{C}+2+\dfrac{C^2l^2\beta\left(l\delta_{12}-\delta_{11}\right)}{D\gamma}$;

$c_1=\dfrac{KC^2l^6\beta\left(5\delta_{11}-4l\delta_{12}\right)}{60D^2\gamma}+\dfrac{2C^2l^3\beta\delta_{12}}{D\gamma}-\dfrac{2C^2l}{\gamma}$;

$c_2=\dfrac{\beta\left(l\delta_{12}-\delta_{11}\right)}{\gamma}\left(Kl^2+2C-\dfrac{C^2l^2}{D}\right)$;

$c_3=\dfrac{C\beta\left(\delta_{11}-l\delta_{12}\right)}{\gamma}$; $c_4=-\dfrac{l^2D_{\mathrm{t}}}{C}$;

$c_5=\dfrac{l^2D_{\mathrm{t}}\beta\left(\delta_{11}-l\delta_{12}\right)}{\gamma}$; $c_6=\dfrac{C^2l^6D_{\mathrm{t}}\beta\left(3l\delta_{12}-4\delta_{11}\right)}{12D^2\gamma}$;

$c_7=\dfrac{Kl^2}{C}+2+\dfrac{\beta}{C}\left(l\delta_{22}-\delta_{12}-\dfrac{l}{K_\theta}\right)$;

$c_8=\beta\left(\delta_{12}-l\delta_{22}-\dfrac{l}{K_\theta}\right)\left(\dfrac{Kl^2+2C}{C^2}-\dfrac{l^2}{D}\right)$;

$c_9=\dfrac{l^3\beta}{D}\left(\delta_{22}+\dfrac{1}{K_\theta}\right)\left(2-\dfrac{Kl^4}{15D}\right)-\dfrac{Kl^2}{C}-2$;

$c_{10}=1-c_8$; $c_{11}=\dfrac{\beta}{C}\left(\delta_{12}-l\delta_{22}-\dfrac{l}{K_\theta}\right)$;

$c_{12}=c_4$; $c_{13}=c_4c_{11}$; $c_{14}=-c_4$; $c_{15}=-c_{13}$;

$c_{16}=\dfrac{l^6\beta D_{\mathrm{t}}}{4D^2}\left(l\delta_{22}-\dfrac{4}{3}\delta_{12}+\dfrac{l}{K_\theta}\right)$;

$c_{17}=Kl^2/C+2$; and

$\gamma=C\left(2Cl+\beta\delta_{11}-l\beta\delta_{12}\right)$.

By substituting the virtual nodal displacements into Eq. (9), the matrix $\boldsymbol{K}_1$, the matrix $\boldsymbol{K}_2$, and the vector $\boldsymbol{Q}_3$ in Eq. (10) are derived as

$$\left.\begin{aligned}
\boldsymbol{K}_1 &= \alpha_1\begin{bmatrix}
C_1 & C_2 & C_3 & C_4 & & & \\
C_5 & C_6 & C_7 & C_8 & & & \\
1 & -4 & 6 & -4 & 1 & & \\
 & \ddots & \ddots & \ddots & \ddots & \ddots & \\
 & & 1 & -4 & 6 & -4 & 1\\
 & & & 1 & -4 & 5 & C_9\\
 & & & & 2 & C_{10} & C_{11}
\end{bmatrix}_{(n+1)\times(n+1)}\\
\boldsymbol{K}_2 &= \alpha_2\begin{bmatrix}
C_{12} & C_{13} & c_2 & c_3 & & \\
1 & -2 & 1 & & & \\
 & \ddots & \ddots & \ddots & & \\
 & & 1 & -2 & 1 & \\
 & & & & C_{14}
\end{bmatrix}_{(n+1)\times(n+1)}\\
\boldsymbol{Q}_3 &= \left\{C_{15},C_{16},0,\cdots,0,C_{17},C_{18}\right\}^{\mathrm{T}}_{1\times(n+1)}
\end{aligned}\right\} \tag{18}$$

where $C_1=c_0c_7+c_8-4c_0+6$;

$C_2=c_1c_7+c_9-4c_1-4$; $C_3=c_2c_7+c_{10}-4c_2+1$;

$C_4=c_3c_7+c_{11}-4c_3$; $C_5=c_0-4$; $C_6=c_1+6$;

$C_7=c_2-4$; $C_8=c_3+1$; $C_9=c_{17}-4$; $C_{10}=-2c_{17}$;

$C_{11}=\left(c_{17}-2\right)^2+2$; $C_{12}=c_0-2$; $C_{13}=c_1+1$;

$C_{14}=c_{17}-2$;

$C_{15}=\alpha_1\left[c_{12}q_{-1}+(c_4c_7+c_{13})q_0+c_{14}q_1+(c_5c_7+c_{15})q_2+(c_6c_7+c_{16})q_{\mathrm{m}}-4(c_4q_0+c_5q_2+c_6q_{\mathrm{m}})\right]-\alpha_2\left(c_4q_0+c_5q_2+c_6q_{\mathrm{m}}\right)$;

$C_{16}=\alpha_1\left(c_4q_0+c_5q_2+c_6q_{\mathrm{m}}\right)$; $C_{17}=-\alpha_1c_{14}q_n$; and

$C_{18}=\alpha_1\left[c_{14}\left(q_{n-1}-q_{n+1}\right)-c_{17}c_{14}q_n+4c_{14}q_n\right]+\alpha_2c_{14}q_n$.

Particularly, when the two ends of the beam model are imposed to free boundary conditions, Eq. (18) can be written as

$$\boldsymbol{K}_1=\alpha_1\begin{bmatrix}C_{11} & C_{10} & 2 & & & & \\ C_9 & 5 & -4 & 1 & & & \\ 1 & -4 & 6 & -4 & 1 & & \\ & \ddots & \ddots & \ddots & \ddots & \ddots & \\ & & 1 & -4 & 6 & -4 & 1 \\ & & & 1 & -4 & 5 & C_9 \\ & & & & 2 & C_{10} & C_{11}\end{bmatrix}_{(n+1)\times(n+1)}$$

$$\boldsymbol{K}_2=\alpha_2\begin{bmatrix}C_{14} & & & & \\ 1 & -2 & 1 & & \\ & \ddots & \ddots & \ddots & \\ & & 1 & -2 & 1 \\ & & & & C_{14}\end{bmatrix}_{(n+1)\times(n+1)}$$

$$\boldsymbol{Q}_3=\{C_{19},C_{20},0,\cdots,0,C_{17},C_{18}\}^{\mathrm{T}}_{1\times(n+1)} \tag{19}$$

where $C_{19}=-\alpha_1 c_{14}q_0$;

and

$$C_{20}=\alpha_1\left[c_{14}\left(q_1-q_{-1}\right)-c_{17}c_{14}q_0+4c_{14}q_0\right]+\alpha_2 c_{14}q_0.$$

2.4 Determination of model parameters

2.4.1 Foundation model parameters

For the Winkler foundation model, the coefficient of subgrade reaction k can be determined according to the estimation method proposed by Wood[26]

$$k=\frac{3E_{\mathrm{s}}}{R\left(1+\nu_{\mathrm{s}}\right)\left(5-6\nu_{\mathrm{s}}\right)} \tag{20}$$

where E_{s} and ν_{s} are Young's modulus and Poisson's ratio of foundation soil, respectively; and R is the radius of the tunnel.

2.4.2 Tunnel model parameters

According to the reference[23], the equivalent longitudinal bending stiffness, $(EI)_{\mathrm{eq}}$ and shear stiffness, $(\kappa GA)_{\mathrm{eq}}$ of the shield tunnel can be calculated as follows:

$$(EI)_{\mathrm{eq}}=E_{\mathrm{c}}I_{\mathrm{c}}\frac{K_{\mathrm{f}}l_{\mathrm{s}}}{K_{\mathrm{f}}\left(l_{\mathrm{s}}-\zeta l_{\mathrm{b}}\right)}=\eta E_{\mathrm{c}}I_{\mathrm{c}} \tag{21}$$

$$K_{\mathrm{f}}=\frac{\cos^3\psi}{\cos\psi+\left(\psi+\pi/2\right)\sin\psi} \tag{22}$$

$$\psi+\cot\psi=\pi\left(\frac{1}{2}+\frac{\lambda nE_{\mathrm{b}}A_{\mathrm{b}}}{E_{\mathrm{c}}A_{\mathrm{c}}}\right) \tag{23}$$

$$(\kappa GA)_{\mathrm{eq}}=\frac{\xi l_{\mathrm{s}}}{\dfrac{l_{\mathrm{b}}}{n\kappa_{\mathrm{b}}G_{\mathrm{b}}A_{\mathrm{b}}}+\dfrac{l_{\mathrm{s}}-l_{\mathrm{b}}}{\kappa_{\mathrm{c}}G_{\mathrm{c}}A_{\mathrm{c}}}} \tag{24}$$

where E_{c} and I_{c} are the Young's modulus and the moment of inertia of the main cross-section of the shield tunnel lining ring segment, respectively; K_{f} is the rotational stiffness coefficient of the joint between rings; ψ represents the location of the neutral axis of the cross-section in the longitudinally bending shield tunnel; l_{s} is the ring width of lining segment; l_{b} is the length of the joint bolt between rings; ζ is the influence coefficient of the joint between rings, which is taken as 0.5 for the shield tunnels of Shanghai Metro suggested by Xu[27]; η is the efficiency of longitudinal bending stiffness; E_{b} is the modulus of elasticity of the joint bolts; ξ is the correction coefficient considering the contact effect between the segment rings; n is the number of joint bolts between rings; κ_{b}=0.89 and κ_{c}=0.53 are shear coefficients of bolt and segment ring, respectively; G_{b} and G_{c} are shear modulus of bolt and segment, respectively; A_{b} and A_{c} are the sectional areas of bolt and segment ring, respectively.

3 Validation by numerical modelling

3.1 Reliability of the analytical solutions

Taking a subway tunnel as an example and referring to the analytical model proposed in the current study, we established a finite element model of one-dimensional elastic foundation beam using ABAQUS. The reliability of the analytical solution proposed in the current study was validated based on the finite element numerical solutions. The numerical model of one-dimensional foundation beam established is shown in Fig. 5. The relevant model parameters can be determined according to the case study by Wu et al.[24]; namely, the outer diameter of the tunnel is 6.2 m, the segment thickness is 0.35 m; the longitudinal length is 100 m; the bending stiffness of the beam (i.e., tunnel) $D=1.361\times10^8$ kN·m^2; the shear stiffness of the beam $C=2.08\times10^6$ kN ($\xi=1$); the coefficient of subgrade reaction k=5 344.4 kN/m^3. The external load is normally distributed. To highlight the influence of the boundary condition at the left end of the model, the external load distribution is assumed as

$$q(x)=490.7\mathrm{e}^{-\left(\frac{x-10}{7.033}\right)^2}\ \left(\mathrm{kN/m}\right) \tag{25}$$

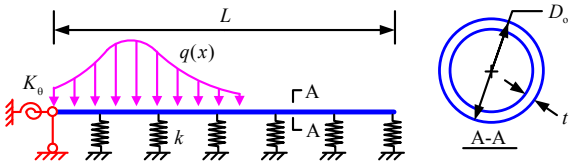

Fig. 5 Schematic illustration for the one-dimensional foundation beam model

Figure 6 shows the comparison between the analytical solutions proposed in the current study and the finite element method-based numerical solutions of the longitudinal deformation and internal forces of the foundation beam when the rotational stiffness of the rotation spring at the left end of the model K_θ is 1.0×10^6 kN·m/rad. It can be seen that the proposed analytical solutions agree well with the finite element method-based solutions regarding the longitudinal deformation and internal forces of the foundation beam, except for those slight discrepancies at the ends of the beam. When K_θ is 1.0×10^6 kN·m/rad, the maximum deflection (absolute value), maximum rotation

angle, maximum bending moment and maximum shear force of the beam obtained from the finite element modelling are 8.13 mm, 29.98°, 7.81×10^3 kN·m, and 1.30×10^3 kN, respectively; those results derived from the proposed analytical solutions are 8.09 mm, 31.19°, 7.98×10^3 kN • m, and 1.37×10^3 kN, respectively. Thus, the relative differences between those numerical results and analytical solutions are 0.49%, 4.04%, 2.18% and 5.38%, respectively. It can be concluded that the proposed analytical solutions in the current study are reliable and can be extended for modelling the longitudinal responses of shield tunnels under complicated boundary conditions.

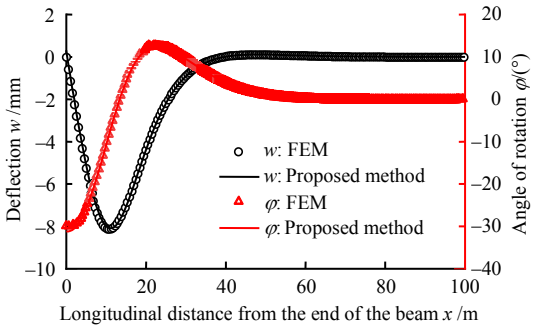

(a) Longitudinal deformation of the beam

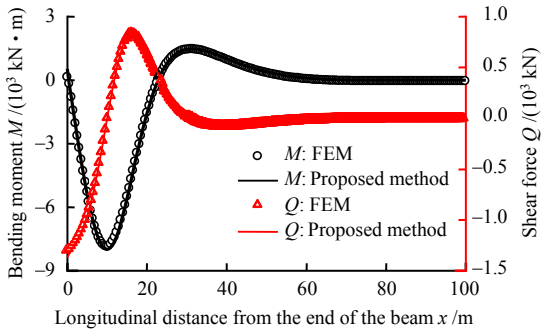

(b) Internal forces of the beam

Fig. 6 Comparison between analytical solutions and FEM-based modelling results

3.2 Applicability of the analytical solutions

In order to justify the applicability of the proposed analytical solution in the current study, the three-dimensional global finite element model was established by the commercial software, ABAQUS for modelling the longitudinal structural response of the shield tunnel caused by the excavation of the foundation pit adjacent to a station (working shaft). The numerical model was used for modelling the interaction between the shield tunnel and the surrounding soils during the excavation of the foundation pit adjacent to the station. The applicability of the proposed analytical model was justified based on the comparison between the three-dimensional finite element modelling results and of the proposed analytical solutions.

3.2.1 Three–dimensional finite element model

The three-dimensional numerical model by ABAQUS is shown in Fig. 7. Fig. 8 shows the relative location between the excavated foundation pit and the existing station-tunnel.

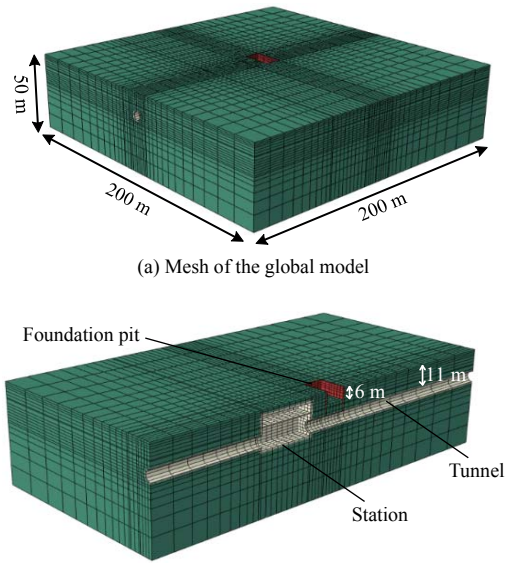

(a) Mesh of the global model

(b) Detailed mesh of the local model

Fig. 7 Three-dimensional numerical model

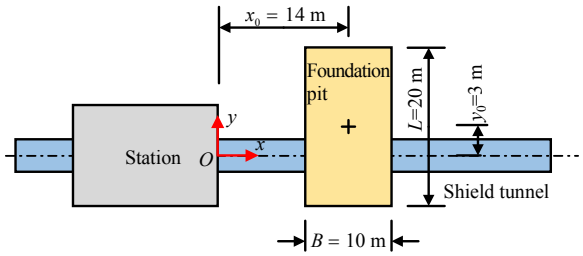

Fig. 8 Relative position between the tunnel-station and the foundation pit

The excavated foundation pit has the dimensions of 10 m (width B) × 20 m (length L) × 6 m (depth H). The distance between the center of the excavated foundation pit and station-tunnel joint is 14 m. The retaining structure for foundation pit is a diaphragm wall with a thickness of 1 m and a depth of 10 m. The underlying tunnel is a typical shield tunnel excavated in a soft soil. The tunnel has an outer diameter of 6.2 m and a segment thickness of 0.35 m. The vertical distance between the top of the tunnel and the bottom of the foundation pit is 5 m. In the numerical model, the C3D8 solid element is used for modeling the stratum, the station, the tunnel as well as the diaphragm wall. The stratum is homogeneous clay layer, which is modelled by modified Cambridge Clay (MCC) model. The model parameters are determined based on the finite element modeling by Kang et al.[9], as shown in Table 1. The underlying tunnel is simulated by the linearly elastic constitutive model. Considering the stiffness reduction caused by the station-tunnel joint, the modulus of elasticity is 2.85 GPa and Poisson's ratio is 0.2[9]. The station and diaphragm wall are also simulated by the linearly elastic constitutive model with the elastic parameters of C30 concrete; namely, the modulus of elasticity is 30 GPa and Poisson's ratio

is 0.2. The numerical model is imposed to constrained normal displacement boundaries except for the free ground surface. In addition, the vertical displacement of the station bottom is constrained in the numerical model, to keep the constraint condition consistent with that in the proposed analytical model at the tunnel-station joint. The rotation stiffness of the rotational spring at the tunnel-station joint is influenced by many factors, the determination of which remains to be studied[24]. In this numerical model, the tunnel and the station are modelled as a whole; namely, the connection is rigid. The influence of the tunnel-station joint on the internal forces and the longitudinal deformation of the shield tunnel will be discussed later. To minimize the boundary effects, the three-dimensional numerical model has the dimensions of 200 m×200 m×50 m. The specific steps of the numerical modeling are as follows. (i) Buildup of the geostress; (ii) construction of the station and the tunnel; and (iii) construction of retaining structure and excavation of the foundation pit. This study focuses on the additional deformation of the existing shield tunnel caused by the excavation of the foundation pit; therefore, the difference in the numerical results between modeling step (ii) and step (iii) should be highlighted.

Table 1 Calculation parameters of the clay soil[9]

γ /(kN·m^{-3})	e_0	K_0	κ	v_s	λ	M
17.8	1.03	0.6	0.013 3	0.3	0.159 4	0.9

Note: γ is the unit weight of the soil; e_0 is the initial void ratio; K_0 is the coefficient of the lateral earth pressure at rest; κ is the slope of the rebound curve; v_s is the Passion's ratio; λ is the slope of the normal compression line; and M is the slope of the critical state line.

3.2.2 Parameters of the analytical model

As shown in Fig. 8, the external load $q(x)$ acting on the longitudinal axis of the tunnel caused by the excavation of the foundation pit can be estimated by Mindlin solution:

$$q(x)=\int_{y_0-(L/2)}^{y_0+(L/2)}\int_{x_0-(B/2)}^{x_0+(B/2)}\frac{\gamma H}{8\pi(1-\nu_s)}\left[-\frac{(1-2\nu_s)(z_0-H)}{R_1^3}+\frac{(1-2\nu_s)(z_0-H)}{R_2^3}-\frac{3(z_0-H)^3}{R_1^5}-\frac{3(3-4\nu_s)z_0(z_0+H)^2-3H(z_0+H)(5z_0-H)}{R_2^5}-\frac{30Hz_0(z_0+H)^3}{R_2^7}\right]\mathrm{d}\chi\mathrm{d}\varsigma \tag{26}$$

where $R_1=\left[(x-\chi)^2+\varsigma^2+(z_0-H)^2\right]^{\frac{1}{2}}$;

$R_2=\left[(x-\varsigma)^2+\varsigma^2+(z_0+H)^2\right]^{\frac{1}{2}}$;

γ and v_s are the unit weight and the Poisson's ratio of the excavated soil, respectively, as shown in Table 1; z_0 and H are the depth of the underlying tunnel axis and the depth of the excavated foundation pit, respectively; x_0 and y_0 are the horizontal distance from the center of the foundation pit to the station and the vertical distance from the center of the foundation pit to the longitudinal axis of the tunnel, respectively; B and L are the width and length of the excavated foundation pit, respectively; and χ and ς are the integral variables along the x direction and y direction in the excavated zone of the foundation pit, respectively.

When modelling the heave of the underlying tunnel induced by the unloading associated with the foundation pit excavation, the rebound modulus of the foundation soil was used[28]. Based on the theoretical model on the one-dimensional soil rebound, Wu et al.[29] proposed a simple method for estimating the rebound modulus at any given point of the base of the foundation pit:

$$E_u=\frac{(\sigma_1-\sigma_2)(1+e_0-\lambda\ln p_1)}{\kappa\ln(p_1/p_2)} \tag{27}$$

where σ_1 and σ_2 are the vertical principal stresses at the studied point before and after excavation, respectively; and p_1 and p_2 are the average principal stresses at the studied points before and after excavation, respectively.

In this case study, the excavation depth of the foundation pit is 6 m and the vertical distance between the top of the tunnel and the bottom of the foundation pit is 5 m. Therefore, when calculating the rebound modulus of the soil according to Eq. (27), the soil depth for calculation can be 8.5 m. By plugging the parameters included in Table 1 into Eq. (27), the rebound modulus of the soil is 8.39 MPa. In addition, the Winkler coefficient of subgrade reaction can be estimated as 1 951.8 kN/m^3 based on Eq. (20).

In the numerical model, the shield tunnel was simulated by a homogeneous continuous model considering the stiffness reduction. The modulus of elasticity with stiffness reduction is 2.85 GPa; and the corresponding bending stiffness and shear stiffness are $D=7.87\times10^7$ kN·m^2 and $C=4.05\times10^6$ kN, respectively.

In the numerical model, the station and tunnel were modelled as a whole finite element model. Thus, the rotation stiffness of the tunnel-station joint was taken as a relatively great value of $K_\theta=1.0\times10^8$ kN·m/rad in the analytical model.

3.2.3 Comparison between analytical solutions and numerical modelling results

Figure 9 shows the comparison between the proposed analytical solutions and the finite element modeling results regarding the additional longitudinal deformation and internal forces of the tunnel. It can be found that the variations of longitudinal deformation, bending moment and shear force of existing tunnels obtained by the proposed analytical model in the current study are consistent with the finite element modelling results.

However, the analytical solutions under the free boundary conditions remarkably deviate from the finite element modelling results for the tunnel near the station. Therefore, it can be concluded that the constraint effect of the tunnel-station joint should be considered when modelling the longitudinal response of the shield tunnels adjacent to the station-tunnel joint. Compared with the existing analytical model with the free boundary assumption, the proposed analytical model in the current study is more applicable to modelling the response of the tunnel induced by the excavation of the foundation pit adjacent to the station.

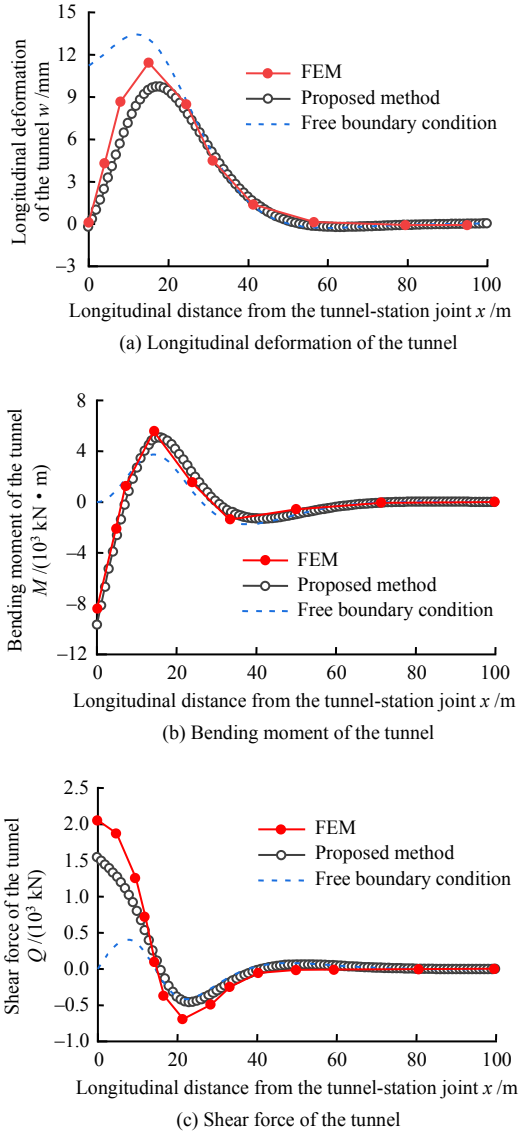

Fig. 9 Comparison between the calculated results by the proposed method and the FEM-based modelling results

According to the modelling results in this case study, the maximal longitudinal deformation, the maximal bending moment and the maximal shear force of the tunnel obtained by the finite element modelling are 11.43 mm, 8 408.0 kN·m and 2 054.4 kN, respectively. Based on the proposed model in the current study, the maximal longitudinal deformation, the maximal bending moment and the maximal shear force of the tunnel are 9.74 mm, 9 651.5 kN • m and 1 543.1 kN, respectively. It shows that the slight discrepancies exist between the modelling results by the proposed analytical model in the current study and those of the finite element method. The main cause can be attribute to the differences in the soil constitutive models; namely, the elastoplastic model, i.e., the MCC model was used in the three-dimensional finite element modelling, while the elasticity theory was used in the proposed analytical model. The heave of the tunnel estimated by the finite element modelling is slightly greater than that by the proposed analytical model. However, as a whole, the proposed analytical model can reproduce the main characteristics of longitudinal deformation of tunnel, and the locations of peak values are consistent with the results by the finite element modelling. Therefore, the applicability of the proposed method under such conditions is justified. Moreover, the proposed analytical solution is more convenient and faster than the three-dimensional finite element modelling.

In addition, it can be found that the maximum bending moment and the maximal shear force of the tunnel occur at the tunnel-station joint. Thus, the joint between the tunnel and the station typically becomes the key location of tunnel, and its connection is vital for the control of the additional response of the tunnel.

4 Discussion

4.1 Effect of rotation stiffness of station-tunnel joint

Figure 10 illustrates that the distribution of additional longitudinal deformation and internal forces along the longitudinal axis of the tunnel, which varies with the rotation stiffness of the station-tunnel joint.

It can be concluded that: (i) as K_θ and the constraint effect of the joint increase, the maximum heave of the tunnel decreases, and the maximum heave approximately occurs at the center of the excavated foundation pit (Fig. 10(a)); (ii) the rotation stiffness of the joint has a great influence on the bending moment, shear force and rotation angle of the tunnel, and the influence zone is mainly in the vicinity of the station-tunnel joint; (iii) as shown in Fig. 10(b), the location of the maximum bending moment of the tunnel gradually moves from the joint to that of the maximum external load (i.e., $x = 14$ m), when the value of K_θ decreases; (iv) as shown in Fig. 10 (c), the shear force at the station-tunnel joint decreases significantly as the value of K_θ decreases, while the shear force near the reverse bending point of the distributed external load (i.e., $x = 19$ m) increases gradually; (v) as illustrated in Fig. 10(d), as the value of K_θ decreases, the distribution pattern of the variation of the rotation angle changes significantly in the vicinity of the station-tunnel joint, and the rotation angle increases significantly at the joint.

Furthermore, based on the modelling results, it can be seen that for the proposed model shown in Fig. 1(b), when the value of K_θ is extremely small, the

station-tunnel joint can be modelled as a vertically simple support; while the joint can be modeled as a fixed support for an extremely large K_θ (i.e., rigid boundary condition).

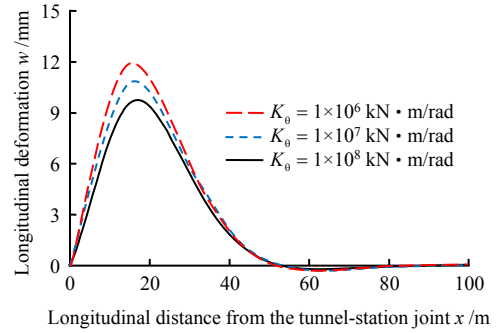

(a) Longitudinal deformation of the tunnel

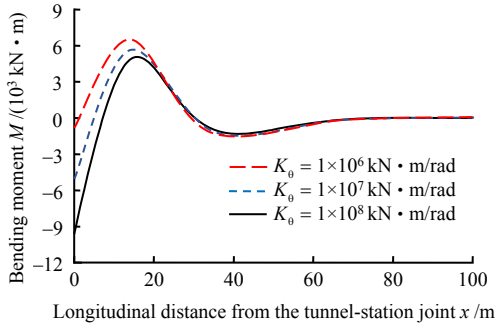

(b) Bending moment of the tunnel

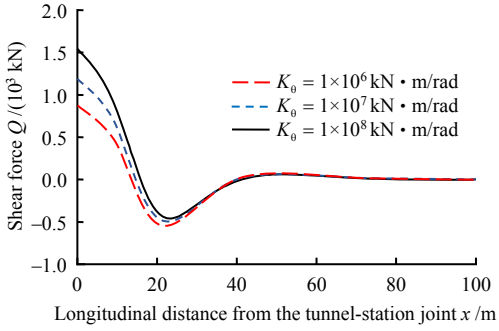

(c) Shear force of the tunnel

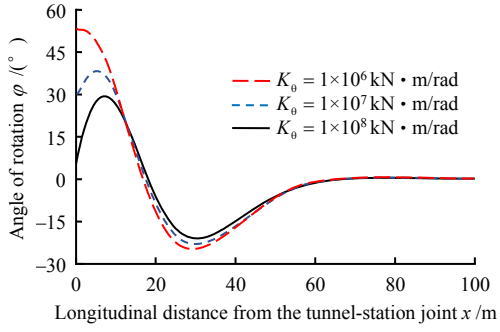

(d) Rotation angle of the cross section of the tunnel

Fig. 10 Effects of the rotation stiffness of the joint between station and tunnel on the internal forces and deformations of the tunnel

Figure 11 depicts the variations of internal forces and rotation angle of the tunnel at the station-tunnel joint with respect to the value of K_θ. In order to facilitate the interpretation, the horizontal axis uses the logarithmic coordinate.

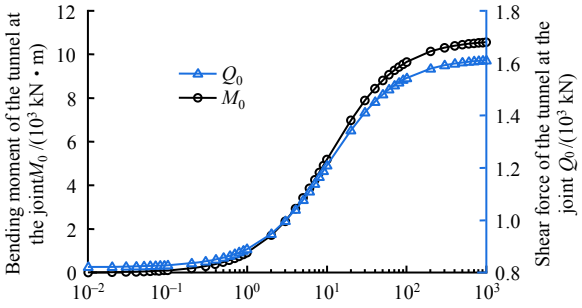

(a) Internal forces of the tunnel at the station-tunnel joint

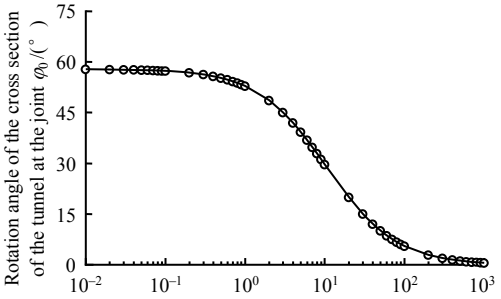

(b) Rotation angle of the cross section of the tunnel at the station-tunnel joint

Fig. 11 The variation of the internal forces and rotation angle of the tunnel at the joint between the station and tunnel with the rotation stiffness of the joint

It can be seen that the bending moment and shear force of the tunnel at the station-tunnel joint increase nonlinearly with the increase in the value of K_θ. When the magnitude of K_θ is relatively small (e.g., less than 10^6 kN•m/rad) or relatively large (greater than 10^8 kN•m/rad), the bending moment and shear force of the tunnel at the joint gradually stabilize. When the magnitude is 10^6 or 10^7 kN•m/rad, the internal forces of the tunnel at the joint increases nonlinearly with the increase in the value of K_θ, and the growth rate increases first and then decreases. In addition, the rotation angle of the tunnel cross-section at the station-tunnel joint varies in an opposite way.

In conclusion, when the station-tunnel joint is less constrained (i.e., a smaller value of K_θ), the values of the additional internal forces are relatively small and the rotation angle is relatively great of the tunnel at the joint. On the other hand, when the station-tunnel joint is more constrained (i.e., a greater value of K_θ), the values of the additional internal forces are relatively great and the rotation angle is relatively small of the tunnel at the joint. It can be found that the station-tunnel joint tends to fail due to the greater constraint and the greater additional internal forces at the joint,

while the smaller constraint is able to accommodate the longitudinal deformation of the tunnel under the additional load. Therefore, it is more advantageous to adopt a more flexible station-tunnel joint regarding the performance of the tunnel at key joints.

4.2 Influence of the plane location of foundation pit

4.2.1 Influence of the relative distance between station and foundation pit

Figure 12 gives the longitudinal deformation and internal forces of the tunnel at different distances from the center of the foundation pit to the station x_0 with the vertical distance between the center of the foundation pit and the axis of the tunnel $y_0 = 0$ (Fig. 8).

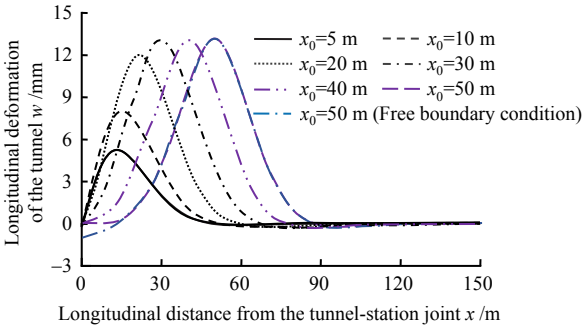

(a) Longitudinal deformation of the tunnel

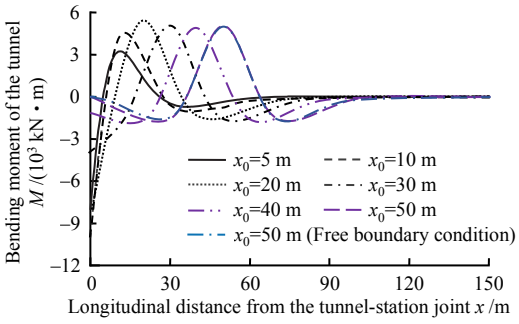

(b) Bending moment of the tunnel

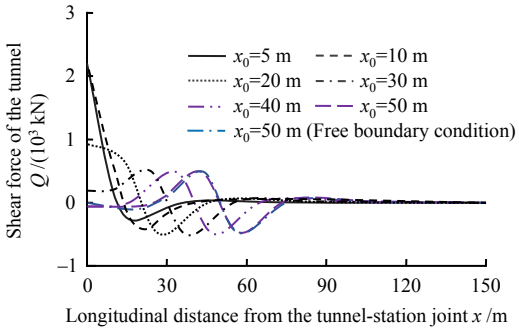

(c) Shear force of the tunnel

Fig. 12 The variation of the deformation and internal forces of the tunnel with the distance between the center of the foundation pit and the station

It can be seen that the maximum longitudinal deformation of the tunnel gradually increases and the maximum bending moment and shear force gradually decrease as the distance between the foundation pit and the station increases. Especially, the bending moment and shear force of the tunnel dramatically change at the station-tunnel connection joint with the increase in x_0. It indicates that when the foundation pit is close to the station, the strong constraint at the joint depresses the longitudinal deformation of the tunnel and induces the remarkable increase in the bending moment and shear force at the joint. Consequently, the excessive bending moment and shear force at the joint can lead to the joint opening and dislocation of the shield tunnel, which will induce water leakage in the tunnel. In addition, when the distance from the center of the foundation pit to the station, $x_0 = 50$ m, the analytical solutions based on the existing model in the free boundary condition agree well with those proposed in the current study on the longitudinal deformation and internal forces. It can be found that the existing model is capable to modeling the mechanical responses of the tunnel when the distance between the foundation pit and the station increases and the constraint effect at the station-tunnel joint weakens. However, the proposed analytical model is more universal in comparison with the existing model.

Figure 13 shows the variations of the bending moment M_0 and the shear force Q_0 of the tunnel at the joint with respect to relative location between the foundation pit and the station x_0 / B in the conditions of different values of rotation stiffness K_θ.

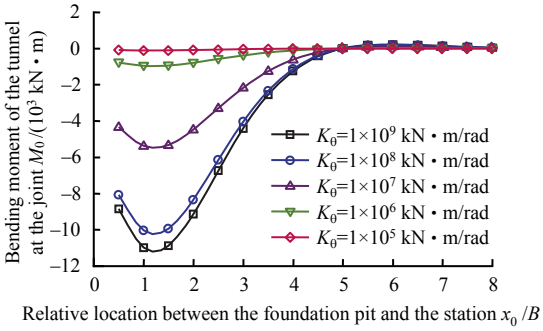

(a) Bending moment of the tunnel at the station-tunnel joint

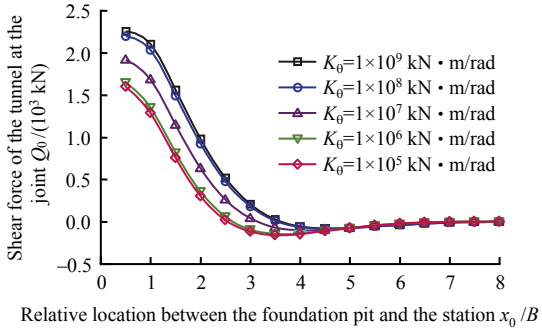

(b) Shear force of the tunnel at the station-tunnel joint

Fig. 13 Relationships between the internal forces of the tunnel at the station-tunnel joint and the relative position of the foundation pit with different values of K_θ

As shown in Fig. 13, as a whole, the bending moment M_0 and the shear force Q_0 decrease when the value of K_θ decreases. When the value of K_θ is

constant, the bending momen M_0 firstly increases and then decreases nonlinearly, and the shear force Q_0 decreases nonlinearly with respect to the value of x_0/B. Moreover, when the value of $x_0/B=5$, both the bending moment M_0 and the shear force Q_0 tends to zero without any significant variations. It indicates that when the value of x_0/B is less than 5, the constraint effect of the station-tunnel joint cannot be neglected and the proposed model in the current study is more capable to evaluating the longitudinal responses of shield tunnel induced by the additional loads.

Figure 14 illustrates the variations of the bending moment M_0 and the shear force Q_0 of the tunnel at the joint with respect to relative location between the foundation pit and the station x_0/B in the conditions of different values of modulus of elasticity of the foundation soil E_s.

As shown in Fig. 14, the variation characteristics of M_0 and Q_0 with respect to relative location between the foundation pit and the station x_0/B in the conditions of different values of E_s agree well with those in the conditions of different values of K_θ. Both M_0 and Q_0 decrease nonlinearly as the value of E_s increases. It indicates that the constraint of the station-tunnel joint has a remarkable effect on the modelling results when the value of x_0/B is less than 4–5. In addition, the influence range decreases slightly with the increase of the foundation stiffness.

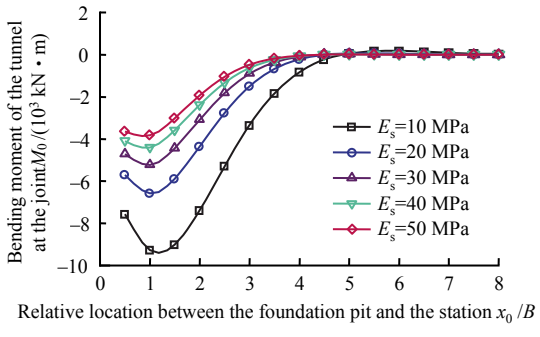

(a) Bending moment of the tunnel at the station-tunnel joint

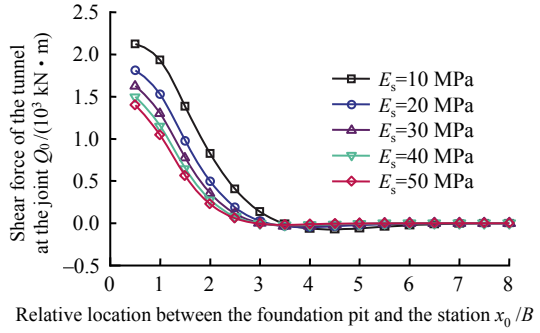

(b) Shear force of the tunnel at the station-tunnel joint

Fig. 14 Relationships between the internal forces of the tunnel at the station-tunnel joint and the relative position of the foundation pit with different values of E_s

Figure 15 demonstrates the variations of the bending moment M_0 and the shear force Q_0 of the tunnel at the joint with respect to relative location between the foundation pit and the station x_0/B in the conditions of different buried depths of the tunnel z_0/H (the buried depth of tunnel axis z_0 and the excavated depth of foundation pit H).

It shows that the influence of excavation of the overlying foundation pit on the underlying tunnel decreases gradually as the buried depth of the tunnel increases. The variation characteristics of M_0 and Q_0 with respect to x_0/B in the conditions of different burial depths of the tunnel z_0/H are similar to those in the conditions of different values of K_θ or E_s; namely, when the value of z_0/H is constant, the bending moment M_0 firstly increases and then decreases nonlinearly, and the shear force Q_0 decreases nonlinearly with respect to the value of x_0/B. It indicates that on the whole, when the distance from the center of the foundation pit to the station exceeds five times the width of the foundation pit (i.e., $x_0/B \geqslant 5$), both M_0 and Q_0 tend to zero gradually without any remarkable variations. It can be concluded that the constraint effect of the station-tunnel joint on the tunnel reduces gradually when x_0/B exceeds 5.

In conclusion, based on the modelling results of the variation of the bending moment and shear force at the station-tunnel joint with respect to relative location between the foundation pit and the station x_0/B in the conditions of different values of K_θ, E_s, or z_0/H, the influence range of the constraint effect of the joint on the tunnel is around 4–5 times the width of the foundation pit. Thus, when the relative location between the foundation pit and the station satisfies this condition, the longitudinal performance of underlying shield tunnel induced by the excavation of the adjacent foundation pit should be evaluated by the proposed analytical model in the current study.

4.2.2 Influence of the relative distance between tunnel and foundation pit

Figure 16 presents the longitudinal deformation and internal forces of the tunnel at different distances from the center of the foundation pit to the tunnel axis, y_0.

As illustrated in Fig. 16, the influence of the foundation pit excavation on the underlying tunnel decreases rapidly with increasing distance between the center of foundation pit and the tunnel axis. When $y_0=30$ m, namely the distance between the center of foundation pit and the tunnel axis is 1.5 times the length of the foundation pit (perpendicular to the tunnel axis), the influence of the foundation pit on the underlying tunnel is not significant.

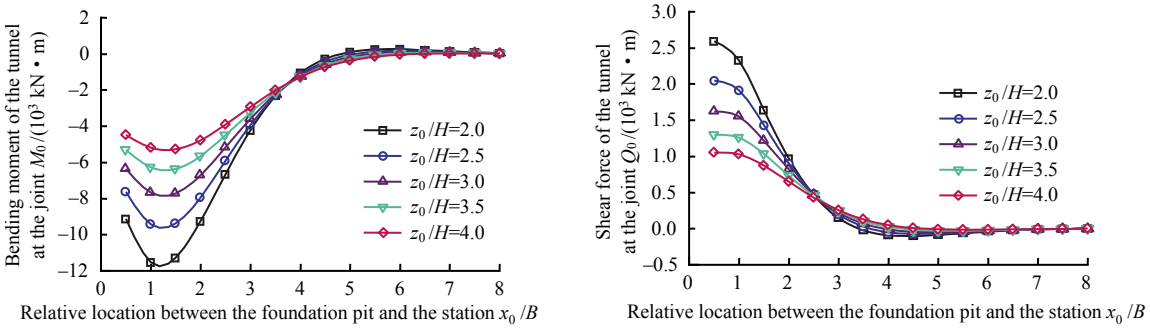

(a) Bending moment of the tunnel at the station-tunnel joint (b) Shear force of the tunnel at the station-tunnel joint

Fig. 15 Relationships between the internal forces of the tunnel at the station-tunnel joint and the relative position of the foundation pit with different buried depths of the tunnel

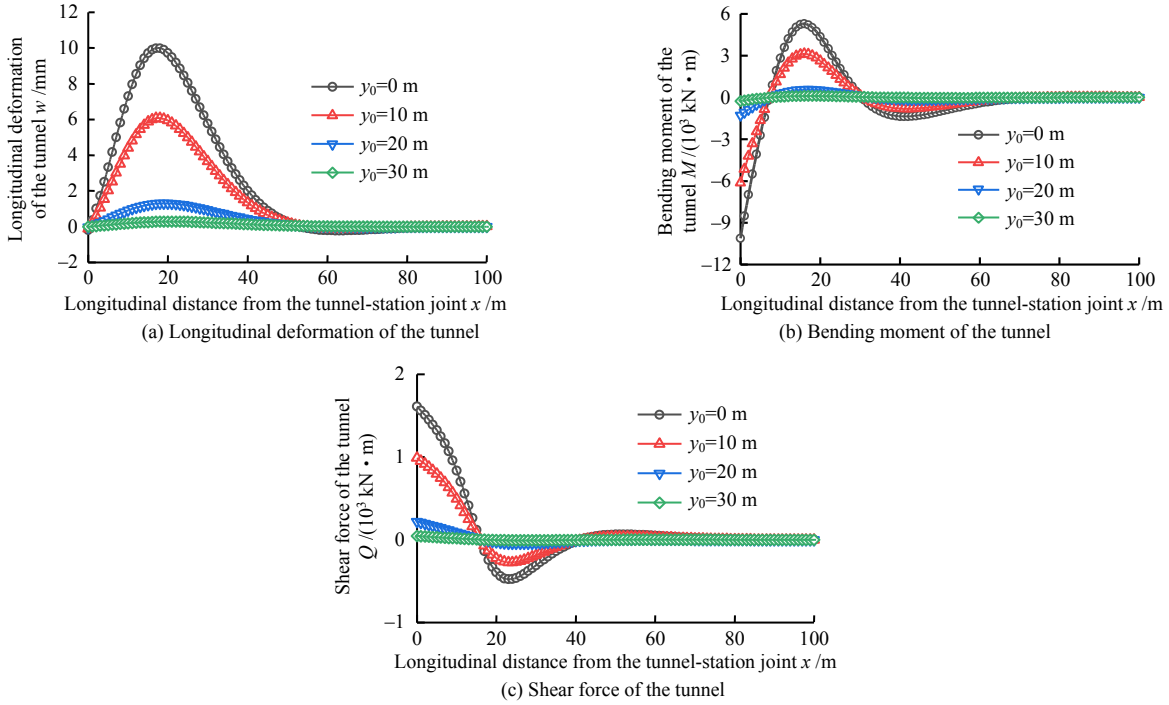

(a) Longitudinal deformation of the tunnel (b) Bending moment of the tunnel

(c) Shear force of the tunnel

Fig. 16 The variation of deformation and internal forces of the tunnel with the distance between the center of the foundation pit and the axis of the tunnel

Furthermore, the influence range of foundation pit excavation on the underlying tunnel is evaluated based on the modelling results of the maximum deformation and maximum internal forces of the tunnel. Fig. 17 shows the variations of maximum deflection w_{max} and maximum internal forces M_{max} and Q_{max} with the relative location between the foundation pit and the tunnel y_0 / L (the length of the foundation pit, L).

As shown in Fig. 17, the maximum deflection and internal forces of the tunnel induced by the excavation of the foundation pit reach the maximum values when the tunnel axis is exactly beneath the foundation pit (i.e., y_0 / L=0). The variations of w_{max}, M_{max} and Q_{max} with the value of y_0 / L show the similar trend; and they decease rapidly with increasing y_0 / L. The maximum deflection and internal forces of the tunnel tend to zero without any remarkable variations when the value of $y_0 / L \geqslant 2.0$. The modelling results indicate that the influence range of foundation pit excavation on the underlying tunnel is around twice the length of foundation pit. When the distance between the tunnel axis and the center of the foundation pit exceeds twice the length of foundation pit, the influence of foundation pit excavation on the underlying tunnel is not significant and can be ignored.

Figures 18 and 19 show the relationships between the maximum longitudinal deformation of the tunnel and the relative location between the tunnel and the foundation pit in the conditions of different modulus of elasticity of the foundation soil and different buried depths of the tunnel, respectively.

It can be found that the maximum longitudinal uplift deformation of tunnel caused by the foundation pit excavation gradually and nonlinearly decreases as the modulus of elasticity of the foundation soil E_s or the relative buried depth of the tunnel y_0 / L increases. When the foundation soil has a relatively small modulus of elasticity and the tunnel has a relatively shallow buried depth, the maximum longitudinal deformation of the tunnel decreases rapidly as the distance between the tunnel axis and the center of the foundation pit increases. The reduction of the maximum

longitudinal deformation becomes less remarkable as the modulus of elasticity of the foundation soil and the buried depth of the tunnel increase.

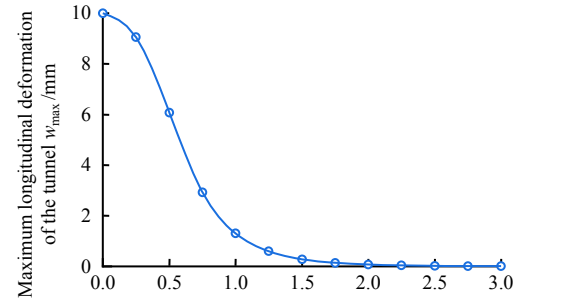

(a) Maximum longitudinal deformation of the tunnel

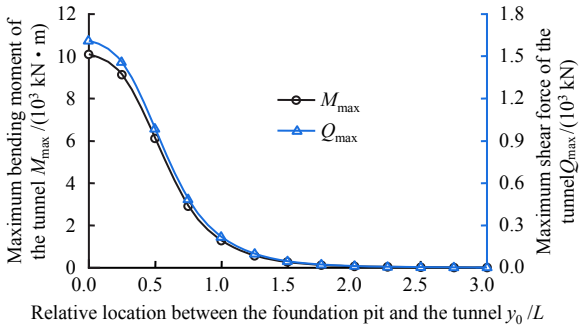

(b) Maximum bending moment and shear force of the tunnel

Fig. 17 Influence of the relative position between the foundation pit and the tunnel on the maximum longitudinal deformation and maximum internal forces of the tunnel

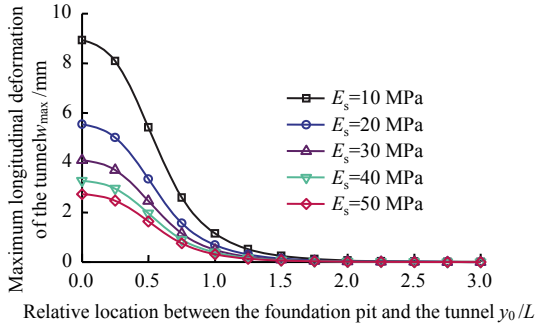

Fig. 18 Relationships between the maximum longitudinal deformation of the tunnel and the relative position between the foundation pit and the tunnel with different values of E_s

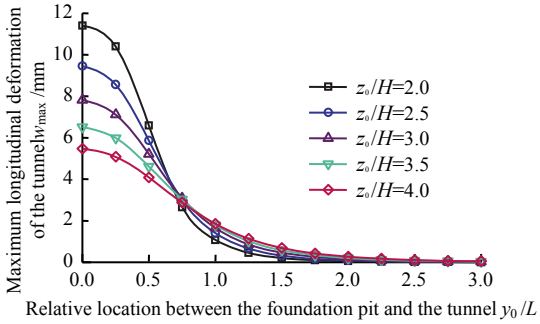

Fig. 19 Relationships between the maximum longitudinal deformation of the tunnel and the relative position between the foundation pit and the tunnel with different depths of tunnel

Based on the parametric studies under multiple working conditions, it can be concluded that the longitudinal deformation of the tunnel becomes less significant, and the maximum deflection tends to zero in the different conditions of foundation soils and buried depths of the tunnel when the distance between the tunnel axis and the center of the foundation pit is greater than twice the length of foundation pit. In other words, in the direction perpendicular to the tunnel axis, the influence range of the excavation of the overlying foundation pit on the underlying tunnel is about twice the length of the foundation pit.

5 Conclusions

An analytical model was proposed in the current study for evaluating the longitudinal deformation of the shield tunnel adjacent to the station (working shaft)-shield tunnel joint. In addition, the finite difference solution to the proposed model was derived. Furthermore, the finite element modelling was conducted to justify the reliability of the proposed model. The main conclusions are summarized as follows:

(1) Based on the basic principles of the force method, the finite difference solution to the governing equations of the Winkler foundation–Timoshenko beam model, which evaluates the longitudinal deformation of the shield tunnel adjacent to station (working shaft) is derived. The proposed modelling result is referable for modelling such problems under complicated boundary conditions.

(2) Based on the finite element modelling results on the one-dimensional elastic foundation beam model and the overall model of the interaction between the shield tunnel and the foundation soil in the condition of the foundation pit excavation adjacent to the station, the reliability and adaptability of the analytical method proposed in the current study was justified for modeling the longitudinal response of the adjacent station (working shaft)–shield tunnel. It indicates that the modelling results of the analytical model proposed in the current study are reliable and applicable to modelling the longitudinal response of the shield tunnel adjacent to a station (working shaft) under the additional loads, e.g., the additional loads induced by the excavation of the foundation pit.

(3) The rotation stiffness of the station-tunnel joint significantly affects the longitudinal deformation and internal forces of the tunnel. The flexible joint between the station and the shield tunnel is more favorable to a good working performance of the shield tunnel at the station-tunnel joint under the additional loads.

(4) The results of parametric studies under multiple working conditions indicate that the constraint effect of the station-tunnel joint on the longitudinal deformation of the tunnel adjacent to the station has a certain influence range, which is around 4–5 times the width of the foundation pit (along the tunnel axis). The excavation of the overlying foundation pit has a remarkable influence on the underlying tunnel when

the distance from the tunnel axis to the center of the foundation pit is shorter than twice the length of the foundation pit (perpendicular to the tunnel axis).

References

[1] HUANG X, HUANG H W, ZHANG J. Flattening of jointed shield-driven tunnel induced by longitudinal differential settlements[J]. Tunnelling and Underground Space Technology, 2012, 31: 20–32.

[2] LIU J W, SHI C H, WANG Z X, et al. Damage mechanism modelling of shield tunnel with longitudinal differential deformation based on elastoplastic damage model[J]. Tunnelling and Underground Space Technology, 2021, 113: 103952.

[3] LEI M F, ZHU B B, GONG C J, et al. Sealing performance of a precast tunnel gasketed joint under high hydrostatic pressures: site investigation and detailed numerical modeling[J]. Tunnelling and Underground Space Technology, 2021, 115: 104082.

[4] HUANG Hong-wei, HUANG Xu, HELMUT S F. Numerical analysis of the influence of deep excavation on underneath existing road tunnel[J]. China Civil Engineering Journal, 2012, 45(3): 182–189.

[5] LIANG Rong-zhu, LIN Cun-gang, XIA Tang-dai, et al. Analysis on the longitudinal deformation of tunnels due to pit excavation considering the tunnel shearing effect[J]. Chinese Journal of Rock Mechanics and Engineering, 2017, 36(1): 223–233.

[6] LIANG R Z, XIA T D, HUANG M S, et al. Simplified analytical method for evaluating the effects of adjacent excavation on shield tunnel considering the shearing effect[J]. Computers and Geotechnics, 2017, 81: 167–187.

[7] LIU Jian-wen, SHI Cheng-hua, LEI Ming-feng, et al. Analytical method for influence analysis of foundation pit excavation on underlying metro tunnel[J]. Journal of Central South University (Science and Technology), 2019, 50(9): 2215–2225.

[8] LIU J W, SHI C H, LEI M F, et al. Improved analytical method for evaluating the responses of a shield tunnel to adjacent excavations and its application[J]. Tunnelling and Underground Space Technology, 2020, 98: 103339.

[9] KANG Cheng, YE Chao, LIANG Rong-zhu, et al. Nonlinear longitudinal deformation of underlying shield tunnels induced by foundation excavation[J]. Chinese Journal of Rock Mechanics and Engineering, 2020, 39(11): 2341–2350.

[10] BAI Xue-feng, WANG Meng-shu. A two-stage method for analyzing the effects of twin tunnel excavation on adjacent tunnels[J]. China Civil Engineering Journal, 2016, 49(10): 123–128.

[11] BAI Xue-feng, WANG Meng-shu. Longitudinal deformation of existing tunnel due to underlying twin-parallel tunnels excavation[J]. China Civil Engineering Journal, 2017, 50(Suppl.1): 123–128.

[12] ZHANG D M, HUANG Z K, LI Z L, et al. Analytical solution for the response of an existing tunnel to a new tunnel excavation underneath[J]. Computers and Geotechnics, 2019, 108: 197–211.

[13] ZHANG Dong-mei, ZONG Xiang, HUANG Hong-wei. Longitudinal deformation of existing tunnel due to underlying shield tunneling[J]. Rock and Soil Mechanics, 2014, 35(9): 2659–2666.

[14] LIU X, FANG Q, ZHANG D L, et al. Behaviour of existing tunnel due to new tunnel construction below[J]. Computers and Geotechnics, 2019, 110: 71–81.

[15] LI Chun-liang, WANG Guo-qiang, ZHAO Kai-jun, et al. Vertical mechnical behavior on shield tunnel under loads on ground surface[J]. Journal of Jilin University (Engineering and Technology Edition), 2011, 41(Suppl.2): 180–184.

[16] KANG Cheng, MEI Guo-xiong, LIANG Rong-zhu, et al. Analysis of the longitudinal deformation of existing shield tunnel induced by temporary surface surcharge[J]. Rock and Soil Mechanics, 2018, 39(12): 4605–4616.

[17] KE Zhai-bang, LIANG Rong-zhu, TONG Zhi-neng, et al. Simplified analytical solution for nonlinear longitudinal deformation of shield tunnels under surface surcharge[J]. Chinese Journal of Geotechnical Engineering, 2019, 41(Suppl.1): 245–248.

[18] CHENG H Z, CHEN R P, WU H N, et al. General solutions for the longitudinal deformation of shield tunnels with multiple discontinuities in strata[J]. Tunnelling and Underground Space Technology, 2021, 107: 103652.

[19] HUANG Yi, HE Fang-she. Beams, plates and shells on elastic foundations[M]. Beijing: Science Press, 2005.

[20] CHENG H Z, CHEN R P, WU H N, et al. A simplified method for estimating the longitudinal and circumferential behaviors of the shield-driven tunnel adjacent to a braced excavation[J]. Computers and Geotechnics, 2020, 123: 103595.

[21] KOIZUMI A, MURAKAMI H, NISHINO K. Study on the analytical model of shield tunnel in longitudinal direction[C]//Proceedings of the Japan Society of Civil Engineers. Tokyo: Publication Committee of Civil Engineering Society, 1988, 9(6): 79–88.

[22] SHIBA Y, KAWASHIMA K, OBINATA N, et al. Evaluation method of longitudinal stiffness of shield tunnel linings for application to seismic response analysis[C]//Proceedings of the Japan Society of Civil Engineers. Tokyo: Publication Committee of Civil Engineering Society, 1989: 385–394.

[23] WU H N, SHEN S L, LIAO S M, et al. Longitudinal structural modelling of shield tunnels considering shearing dislocation between segmental rings[J]. Tunnelling and Underground Space Technology, 2015, 50: 317–323.

[24] WU H N, SHEN S L, YANG J, et al. Soil-tunnel interaction modelling for shield tunnels considering shearing dislocation in longitudinal joints[J]. Tunnelling and Underground Space Technology, 2018, 78: 168–177.

[25] TIMOSHENKO S P, LX V I. On the correction for shear of the differential equation for transverse vibrations of prismatic bars[J]. Philosophical Magazine, 1921, 41(245): 744–746.

[26] WOOD A M M. The circular tunnel in elastic ground[J]. Geotechnique, 1975, 25(1): 115–127.

[27] XU Ling. Study on longitudinal settlement of shield tunnel in soft soil[D]. Shanghai: Tongji University, 2005.

[28] HUANG Xu, HUANG Hong-wei, ZHANG Dong-mei. Longitudinal deflection of existing shield tunnels due to deep excavation[J]. Chinese Journal of Geotechnical Engineering, 2012, 34(7): 1241–1249.

[29] WU Hao, WANG Yi-jun, WANG Hai, et al. Simplified calculation method for rebound of large area foundation pit excavation[J]. China Civil Engineering Journal, 2020, 53(Suppl.1): 361–366.